Missouri University of Science and Technology

Scholars' Mine

International Specialty Conference on Cold-Formed Steel Structures

(2012) - 21st International Specialty Conference on Cold-Formed Steel Structures

Aug 24th, 12:00 AM - Aug 25th, 12:00 AM

Compression-tension Hysteretic Response of Cold-formed Steel C-stection Framing Members

D. Padilla-Llano

C. D. Moen

M. Eatherton

L. McAnallen

T. Bruce

Follow this and additional works at: https://scholarsmine.mst.edu/isccss

 Part of the Structural Engineering Commons

Recommended Citation

Padilla-Llano, D.; Moen, C. D.; Eatherton, M.; McAnallen, L.; and Bruce, T., "Compression-tension Hysteretic Response of Cold-formed Steel C-stection Framing Members" (2012). *International Specialty Conference on Cold-Formed Steel Structures*. 5.
https://scholarsmine.mst.edu/isccss/21iccfss/21iccfss-session2/5

This Article - Conference proceedings is brought to you for free and open access by Scholars' Mine. It has been accepted for inclusion in International Specialty Conference on Cold-Formed Steel Structures by an authorized administrator of Scholars' Mine. This work is protected by U. S. Copyright Law. Unauthorized use including reproduction for redistribution requires the permission of the copyright holder. For more information, please contact scholarsmine@mst.edu.

Twenty-First International Specialty Conference on Cold-Formed Steel Structures
St. Louis, Missouri, USA, October 24 & 25, 2012

Compression-Tension Hysteretic Response of Cold-Formed Steel C-Section Framing Members

D. Padilla-Llano[1], C. D. Moen[2], M. Eatherton[3], L. McAnallen[4], T. Bruce[5]

Abstract

This paper summarizes results from an experimental program designed to evaluate the tension-compression cyclic axial response of cold-formed steel C-section structural framing members. A new cyclic loading protocol for cold-formed steel members is presented that defines the target axial displacement based on elastic buckling parameters. The protocol is used to explore the cyclic response of members experiencing local buckling, distortional buckling, and global buckling deformation. In the experiments, post-bucking energy dissipation was observed along with tension stretching and softening. The quantity of dissipated energy per cycle increased as cross-section and global slenderness decreased. Specimens experiencing local and distortional buckling dissipated more energy per half-wavelength than those experiencing global buckling.

Introduction

Current seismic analysis and design procedures for mid-rise cold-formed steel frame buildings focuses on the lateral force resisting system (AISI S213 2007), e.g., shear walls constructed with perimeter-cold formed steel members sheathed with Structural 1 plywood (4 ply), oriented strand board (OSB), gypsum board, or thin sheet steel or strap bracing. These subsystems are strategically distributed throughout a building to provide lateral stiffness during a wind event and to dissipate energy and limit residual lateral drift during a seismic event.

[1] Graduate Research Assistant, Virginia Tech, dapadill@vt.edu
[2] Assistant Professor, Virginia Tech, cmoen@vt.edu
[3] Assistant Professor, Virginia Tech, meather@vt.edu
[4] Undergraduate Research Assistant, Virginia Tech, lem421@vt.edu
[5] Undergraduate Research Assistant, Virginia Tech, btrevor@vt.edu

A seismic design parameter typically available to a designer of cold-formed steel framed building is the experimentally obtained subsystem seismic response modification coefficient (R) that reduces the elastic demand forces based on stiffness changes during a seismic event, e.g., Boudreault et al. (2007). However, specific guidance about stiffness or strength degradation and energy dissipation are not readily available. Additionally, there is very little known about hysteretic behavior of the subsystem components or connections (e.g., drag struts, boundary chord studs), which limits our ability to perform nonlinear dynamic time history analysis of a cold-formed steel framed building with phenomenological models, e.g., Fig. 1.

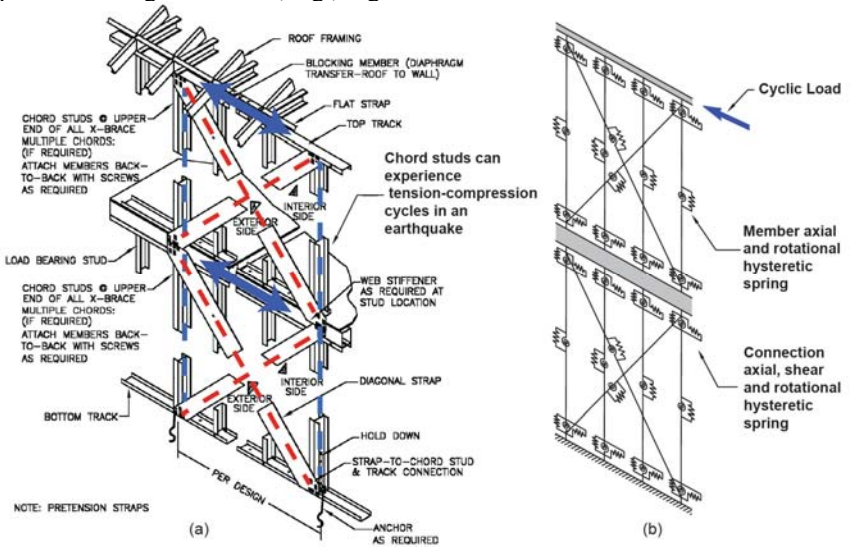

Figure 1. Cold-formed (a) strap bracing; and (b) corresponding phenomenological model

The goal of the research summarized in this paper is to focus on cold-formed steel component cyclic behavior, and specifically axial compression-tension hysteretic response. The study focuses on common C-section cold-formed steel framing members. Experiments are conducted that accommodate performance comparisons for different compression limit states – local buckling, distortional buckling, and global buckling. This research is motivated by a larger National Science Foundation NEES research initiative to integrate modern thin-walled analysis tools with existing performance-based design approaches that will improve the seismic design of cold-formed steel framing systems (Schafer et al. 2012).

Background - hysteretic response including buckling

Hysteretic response of axial members has been studied in detail with regard to hot-rolled steel framed buildings and offshore oil platforms, and so before describing our specific experimental program, it worthwhile to introduce some of the existing literature related to hysteretic response and buckling.

The study of globally slender axial steel member cyclic behavior (struts, braces) began in the early 1970s with analytical derivations and experimental programs. Analytical hysteretic response models for columns experiencing a plastic hinge were developed so that they could be input into finite element building models (Higginbotham and Hanson 1976; Ikeda and Mahin 1986; Goel and Tang 1987; Papadrakakis and Loukakis 1987). Some of the models included cross-sectional slenderness as a softening parameter (Nonaka 1973; Sohal and Chen 1987). The analytical models were combined with experimental data in a few cases to develop semi-empirical equations that predict bracing member fracture life, i.e., number of cycles to tensile fracture (Goel 1992).

The viability of these analytical models was established by several experimental programs ranging from solid steel bars (e.g., Higginbotham and Hanson 1976) to hollow thin-walled tubes (Goggins et al. 2006), W-sections (Popov and Black 1981) and angles (Jain et al 1980). A few experiments even considered the influence of cold-bending on energy dissipation (Popov et al. 1979). The important conclusions from these studies were that members always stretched in tension and that this stretching can be predicted (Jain et al 1980); that tension capacity remained constant before fracture but compression capacity degraded with the number of cycles; and when local buckling accompanied global deformation, typically the member failure mode was tensile fracture caused by stress concentrations at a fold.

It was also observed in the experimental studies that inelastic behavior was the key contributor to energy dissipation when compared to inherent material damping, that total energy dissipation was independent of loading direction (tension then compression or compression and then tension) and that the amount of hysteretic energy dissipated decreases as the global slenderness increases. A goal of our research is to understand if this slenderness trend holds true for local or distortional buckling slenderness. Only a few studies have focused on energy dissipation from local buckling (Yao and Nikolov 1992; Usami and Ge 1998; Watanabe et al 1992; Calderoni et al. 2009). It was observed that local buckling compression capacity degraded to a constant magnitude with increasing cycles, which is different than global buckling cyclic behavior where compression capacity goes to zero as the plastic hinge develops.

Experimental program design

An experimental program was conducted to study the response of cold-formed steel lipped channels subjected to cyclic axial load. The test program includes two quasi-static cyclic tests and two monotonic tests per specimen type. The monotonic tests were performed to establish an envelope and backbone for comparison to the cyclic response and determine strength degradation parameters.

Specimen selection strategy

Specimens were selected such that their predicted monotonic capacity in compression is governed either by local, distortional or global buckling as predicted by the AISI Direct Strength Method (AISI 2007). The cross-sections considered were selected from the Structural Stud Manufacturers Association catalog (SSMA 2011). Cross-section dimensions and length were varied to isolate each limit state. Two different web depths (92mm and 152 mm) were selected. The test matrix is summarized in Table 1 (with nominal dimensions) and specimen nomenclature is explained in Fig. 2a.

Specimen dimensions, material properties and elastic buckling loads

Cross-section dimensions were measured at member mid-height using methods described in Moen (2008), see Table 2. These values were used to calculate the elastic buckling loads ($P_{cr\ell}$, P_{crd}, P_{cre}), and the half-wavelength ($L_{cr\ell}$, L_{crd}) with finite strip eigen-buckling analysis in CUFSM (Ádány and Schafer 2006). The yield load P_y was determined using the measured cross-section area and the average yield stress obtained from three coupon tests per specimen – one coupon from each flange and one from the web – conducted in accordance with ASTM E8M-04 (ASTM 2004). The monotonic compression capacity, P_n, was calculated using the AISI Direct Strength Method (AISI 2007). These values are summarized in Table 3.

Table 1. Test Matrix with nominal dimensions and the number of tests

Specimen	Limit State	L (mm)	Web Depth (mm)	Flange Width (mm)	Thickness (mm)	No. of Cyclic Tests	No. of Monotonic Tests
362S162-54-LA#	Local	305	92	41	1.44	2	2
600S162-33-LA#	(λ_ℓ>>λ_d, λ_e)	305	152	41	0.88	2	2
362S137-68-DA#	Distortional	610	92	35	1.81	2	2
600S137-68-DA#	(λ_d>>λ_ℓ, λ_e)	610	152	35	1.81	2	2
362S137-68-GA#	Global	2286	92	35	1.81	2	2
600S137-97-GA#	(λ_e>>λ_ℓ, λ_d)	2286	152	35	2.58	2	2

A= Axial, G= Global, D= Distortional, L= Local, # indicates Cyclic or Monotonic

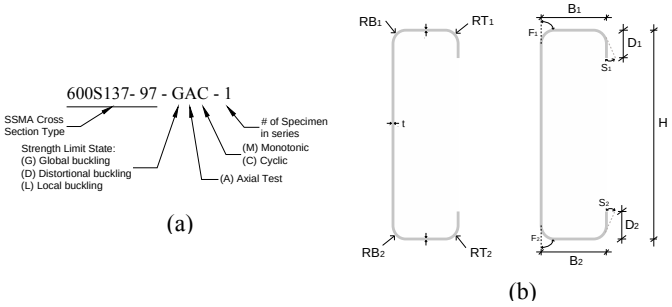

Figure 2. Specimen (a) naming notation; and (b) cross-section dimension

Table 2. Measured specimen dimensions

Specimen	L	A_g	D_1	D_2	B_1	B_2	H	RT_1	RB_1	RT_2	RB_2	F_1	F_2	S_1	S_2
	(mm)	(mm^2)	(mm)	(mm)	(mm)	(mm)	(mm)	(mm)	(mm)	(mm)	(mm)	(°)	(°)	(°)	(°)
600S137-97-GAM-1	2286	631	19.1	17.3	36.2	35.8	152.7	5.2	5.8	4.8	5.2	84.1	89.3	1.7	1.6
600S137-97-GAM-2	2286	632	19.1	17.5	36.1	35.7	152.2	5.0	6.0	4.8	5.2	83.8	87.9	1.6	1.9
600S137-97-GAC-1	2286	634	17.6	19.5	35.8	36.0	152.1	4.8	5.6	4.8	5.4	87.6	84.3	1.0	1.4
600S137-97-GAC-2	2286	629	17.6	18.9	35.6	35.9	152.5	4.8	5.2	5.2	6.0	87.6	85.1	3.1	2.0
362S137-68-GAM-1	2286	315	11.6	13.4	34.5	33.5	93.3	4.0	4.0	4.4	4.4	88.4	87.6	-2.5	4.8
362S137-68-GAM-2	2286	316	11.7	13.5	34.5	33.3	93.2	4.0	3.8	4.4	4.4	86.6	87.8	-3.5	3.6
362S137-68-GAC-1	2286	315	11.8	13.3	34.4	33.6	93.3	4.0	4.0	4.4	4.4	86.6	88.1	-2.0	3.4
362S137-68-GAC-2	2286	315	11.8	13.3	34.4	33.4	93.3	4.0	4.0	4.4	4.4	88.5	88.2	-2.5	4.1
600S137-68-DAM-1	610	416	10.9	11.5	34.8	33.8	152.7	4.0	3.6	4.4	4.2	90.5	88.6	-1.5	0.6
600S137-68-DAM-2	610	415	10.7	11.5	34.8	33.8	152.7	4.0	4.0	4.4	4.0	90.5	89.5	-1.4	-0.7
600S137-68-DAC-1	610	416	10.8	11.3	34.4	34.2	152.7	4.0	4.0	4.2	4.0	91.9	88.1	-1.1	5.0
600S137-68-DAC-2	610	415	10.5	11.9	34.9	33.8	152.5	4.0	4.0	4.4	4.2	89.9	89.6	-1.1	-0.1
362S137-68-DAM-1	610	318	11.9	13.4	34.8	33.5	94.0	4.0	4.0	4.4	4.4	88.8	86.9	-4.7	5.4
362S137-68-DAM-2	610	317	12.0	12.9	34.5	33.9	93.3	4.0	4.0	4.4	4.4	89.8	86.4	-2.0	4.2
362S137-68-DAC-1	610	313	11.5	13.2	34.5	33.5	93.2	4.0	4.0	4.4	4.4	87.6	88.1	-2.3	4.1
362S137-68-DAC-2	610	314	11.6	13.4	34.4	33.9	93.2	4.0	4.0	4.4	4.4	89.7	86.2	-2.1	4.0
600S162-33-LAM-1	305	215	12.9	13.6	42.1	41.7	149.9	3.6	4.2	3.4	4.4	84.4	90.7	5.2	1.6
600S162-33-LAM-2	305	215	13.0	13.5	42.0	41.5	150.3	3.6	4.0	3.6	4.4	88.1	91.9	2.0	-0.2
600S162-33-LAC-1	305	215	12.7	13.6	41.9	41.7	150.6	3.6	4.0	3.6	4.4	84.6	91.1	6.0	1.5
600S162-33-LAC-2	305	215	12.7	13.6	41.9	41.5	150.3	3.6	4.0	3.2	4.4	86.6	89.1	3.1	3.6
362S162-54-LAM-1	305	272	12.0	11.6	41.6	42.3	93.1	3.6	4.4	4.2	4.4	90.2	89.8	0.9	2.4
362S162-54-LAM-2	305	273	11.7	12.2	42.3	41.6	92.7	4.2	4.4	3.6	4.4	89.2	89.2	3.2	2.2
362S162-54-LAC-1	305	272	11.7	11.8	42.0	41.6	92.7	4.0	4.4	3.6	4.4	88.9	89.5	1.0	2.0
362S162-54-LAC-2	305	273	11.8	12.0	42.3	41.7	92.9	4.2	4.4	3.8	4.4	89.0	89.2	5.1	2.3

Test setup and instrumentation

A uniaxial loading frame was assembled to perform the cyclic tests (see Fig. 3). Two end plates were welded to both ends of the specimens to transfer axial forces while providing boundary conditions that were rotation fixed and longitudinal warping fixed. The axial deformations were measured using two LVDT transducers connected between the top and bottom end plates as seen in the right of Fig. 3. This arrangement accommodates an accurate measurement of

the axial displacement without the influence of the end plate deformation (especially when the specimen is in tension).

The specimens were subjected to a cyclic displacement history using a servovalve-controlled hydraulic actuator at a constant displacement rate of 0.008(mm/min)/(mm of specimen length). Based on previous monotonic tension tests (Moncarz and Krawinkler 1981), it is expected that this displacement rate will produce strengths within an approximate range between 2% larger than the static value and 5% smaller than expected earthquake displacement rates, while producing an average test time of 90 minutes. The displacement rate for the monotonic tests was $1x10^{-4}$ (mm/min)/(mm of specimen length) which corresponds to the maximum rate of 21MPa per minute recommended in the AISI test method for column distortional buckling (AISI 2008).

Additional instrumentation – 8 to 16 string potentiometers and 750 to 1800 photogrammetry targets – were provided to capture cross-sectional deformations and analyse the contribution of each buckling mode to the response of the specimens. The data related to this instrumentation will be discussed in a future paper.

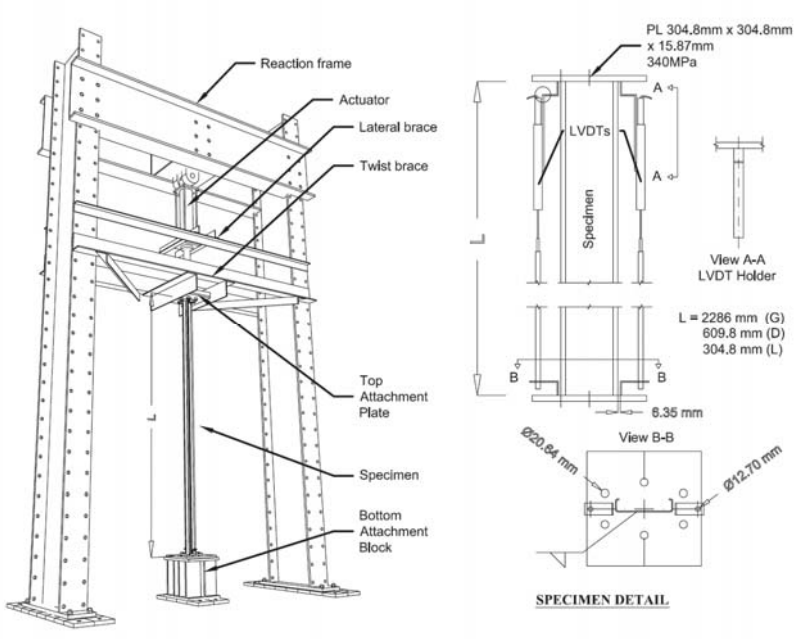

Figure 3. Test setup and specimen detail

Table 3. Elastic buckling properties and predicted compressive capacity

Specimen	P_y (kN)	P_n (kN)	P_{cre} (kN)	λ_e	P_{crd} (kN)	λ_d	L_{crd} (mm)	$P_{crℓ}$ (kN)	$\lambda_ℓ$	$L_{crℓ}$ (mm)	δ_e ($\times 10^{-3}$ mm)
600S137-97-GAM-1	245	121	147	1.29	228	1.04	314	198	0.78	119	654
600S137-97-GAM-2	249	122	147	1.30	232	1.04	314	201	0.78	118	653
600S137-97-GAC-1	242	121	147	1.28	233	1.02	318	202	0.78	118	650
600S137-97-GAC-2	244	120	145	1.30	225	1.04	315	196	0.78	119	647
362S137-68-GAM-1	123	60	71	1.32	165	0.86	253	130	0.68	71	636
362S137-68-GAM-2	122	59	70	1.32	167	0.86	252	131	0.67	71	624
362S137-68-GAC-1	123	59	70	1.32	166	0.86	254	130	0.67	71	626
362S137-68-GAC-2	121	60	71	1.30	165	0.86	254	130	0.68	71	638
600S137-68-DAM-1	177	91	1249	0.38	76	1.53	260	62	1.64	123	173
600S137-68-DAM-2	177	90	1243	0.38	75	1.53	258	62	1.64	124	172
600S137-68-DAC-1	177	91	1270	0.37	76	1.53	259	62	1.64	124	172
600S137-68-DAC-2	177	91	1256	0.38	76	1.53	259	62	1.64	123	173
362S137-68-DAM-1	124	103	968	0.36	180	0.83	256	130	0.95	72	533
362S137-68-DAM-2	123	103	961	0.36	180	0.83	255	132	0.94	71	537
362S137-68-DAC-1	122	101	933	0.36	175	0.83	252	128	0.95	71	529
362S137-68-DAC-2	122	102	947	0.36	177	0.83	254	128	0.95	71	531
600S162-33-LAM-1	72	27	4138	0.13	62	1.08	515	8	3.04	111	32
600S162-33-LAM-2	72	32	4307	0.13	53	1.16	462	11	2.49	108	48
600S162-33-LAC-1	72	27	4125	0.13	60	1.09	512	8	3.05	112	32
600S162-33-LAC-2	72	27	4147	0.13	60	1.09	511	8	3.05	111	32
362S162-54-LAM-1	113	81	3704	0.17	157	0.85	330	70	1.26	72	232
362S162-54-LAM-2	113	81	3674	0.18	160	0.84	333	71	1.26	71	234
362S162-54-LAC-1	113	81	3626	0.18	157	0.85	328	70	1.26	71	233
362S162-54-LAC-2	113	81	3683	0.18	158	0.85	332	70	1.26	72	232

$\lambda_e = (P_y/P_{cre})^{0.5}$; $\lambda_d = (P_y/P_{crd})^{0.5}$; $\lambda_ℓ = (P_{ne}/P_{crℓ})^{0.5}$.

Loading protocol

Cyclic loading protocols are used to experimentally assess the inelastic demand, cumulative damage, and peak displacement demand of a system (or component) associated with a design seismic event (Krawinkler 2009). The axial demand in a cold-formed steel member depends on many factors such as the location of the member in the building or structural system, end connections, ground motion properties, and the building's dynamic properties. The loading protocol developed here (Fig. 4) is focused on characterizing hysteretic behavior and associated progression of damage states in the member rather than reproducing seismic demands for a specific systems or configurations.

The loading protocol was adapted from the FEMA 461 quasi-static cyclic deformation-controlled testing protocol (FEMA 2007). The FEMA 461 loading protocol intends to simulate the cycles leading up to a peak deformation, rearranged in order of increasing amplitude. Using a symmetric protocol with equal deformation demands in compression and tension captures the damage and energy dissipation from cross-sectional deformation of the thin-walled channel sections under compression and damage and tearing that can occur by the

reversal of these deformations under tension loading. There are two cycles per deformation step in the proposed protocol.

The loading protocol anchor point is the elastic axial displacement, δ_e, corresponding to a load P_e that is expected to initiate buckling deformation in the member

$$\delta_e = \frac{P_e L}{AE} \tag{1}$$

This load P_e is calculated using slenderness limits defined in the AISI Direct Strength Method. The DSM approach dictates that local buckling initiates at λ_ℓ=0.776 and the distortional buckling initiates at λ_d=0.561. Using $\lambda=(P_e/P_{cr})^{0.5}$, then $P_e=0.60P_{cr\ell}$ and $P_e=0.31P_{crd}$. The load that initiates global buckling deformation is assumed to be $P_e=0.50P_{cre}$.

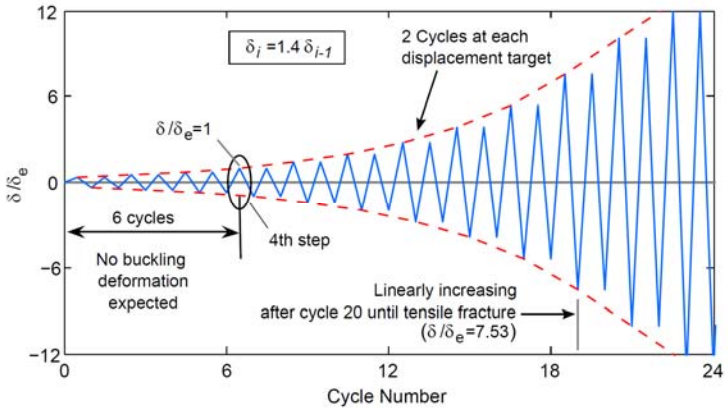

Figure 4. Cyclic compression-tension cold-formed steel loading protocol

Experimental Results

Cyclic and monotonic (compression) load-deformation response was recorded for specimens experiencing local, distortional, and global buckling limit states. From the monotonic tests the average ratio of test peak load to predicted load P_{min}/P_n was 1.00 with a coefficient of variation of 0.09 (see Table 4). This result validates the experimental setup and boundary conditions provided. Specimen cyclic response is asymmetric due to the presence of buckling deformation in compression as shown in Figs. 5 to 7 and strength degradation in compression is quantified with the monotonic response (Figs. 8 to 10). Stiffness and strength in compression is sensitive to cross-section deformations. Additional details for each of the limit states are discussed below and test videos are available on Virginia Tech's digital repository (VTechWorks 2012).

Table 4. Test maximum loads.

Specimen	P_{max} (kN)	δ_{Pmax} ($\times 10^{-3}$mm)	P_{min} (kN)	δ_{Pmin} ($\times 10^{-3}$mm)	P_{max}/P_y	P_{min}/P_n
600S137-97-GAM-1	-	-	-117	-2413	-	0.97
600S137-97-GAM-2	-	-	-101	-2921	-	0.83
600S137-97-GAC-1	236	8890	-129	-2362	0.98	1.06
600S137-97-GAC-2	237	16180	-127	-2388	0.97	1.06
362S137-68-GAM-1	-	-	-56	-2718	-	0.94
362S137-68-GAM-2	-	-	-53	-2362	-	0.90
362S137-68-GAC-1	122	8331	-50	-2464	1.00	0.84
362S137-68-GAC-2	123	9068	-49	-2261	1.01	0.83
600S137-68-DAM-1	-	-	-97	-1829	-	1.07
600S137-68-DAM-2	-	-	-97	-1626	-	1.08
600S137-68-DAC-1	175	3226	-96	-1295	0.99	1.06
600S137-68-DAC-2	174	2769	-100	-1118	0.98	1.10
362S137-68-DAM-1	-	-	-100	-1778	-	0.96
362S137-68-DAM-2	-	-	-98	-1499	-	0.95
362S137-68-DAC-1	127	5512	-99	-1168	1.05	0.98
362S137-68-DAC-2	128	5766	-96	-991	1.05	0.94
600S162-33-LAM-1	-	-	-31	-406	-	1.12
600S162-33-LAM-2	-	-	-33	-559	-	1.04
600S162-33-LAC-1	66	838	-29	-457	0.92	1.06
600S162-33-LAC-2	67	991	-32	-457	0.94	1.19
362S162-54-LAM-1	-	-	-88	-813	-	1.08
362S162-54-LAM-2	-	-	-86	-889	-	1.05
362S162-54-LAC-1	109	1295	-88	-508	0.97	1.08
362S162-54-LAC-2	110	1270	-90	-635	0.97	1.11

P_{max}, P_{min} = test maximum tension and compression respectively.

Global buckling limit state

The GAC specimens exhibited weak axis flexural buckling which led to folding of the stiffening lips near the mid-height as shown in Fig. 5d. Web buckling occurred at the points of reversed curvature near the supports. Damage due to reversal of the strains accumulated at the folded lips as subsequent excursions in tension and compression took place. The compression strength as well as unloading stiffness on the compression side degraded rapidly after the peak compressive load was reached as shown in Fig. 5(b-c). Excursions in tension are characterized by very low stiffness until the member straightens out, then ductile yielding at a consistent tension yield capacity. The final failure mode was gradual tearing of the section starting at the folded lips and propagating through the cross section, or in some cases fracture near the welded connection.

The monotonic responses were also characterized by weak axis flexural buckling, with folding of the stiffening lips at mid-height. Specimen 362S137-68-GAM-2 exhibited flexural-torsional buckling due to torsional initial

imperfections in the member. This resulted in a higher peak compression load and higher monotonic envelope as shown in Fig. 8a and Table 4. The peak compression load of specimen 600S137-97-GAM-2 was reduced by 17% compared to the others due to large initial global imperfections in the weak axis direction (Fig. 8b).

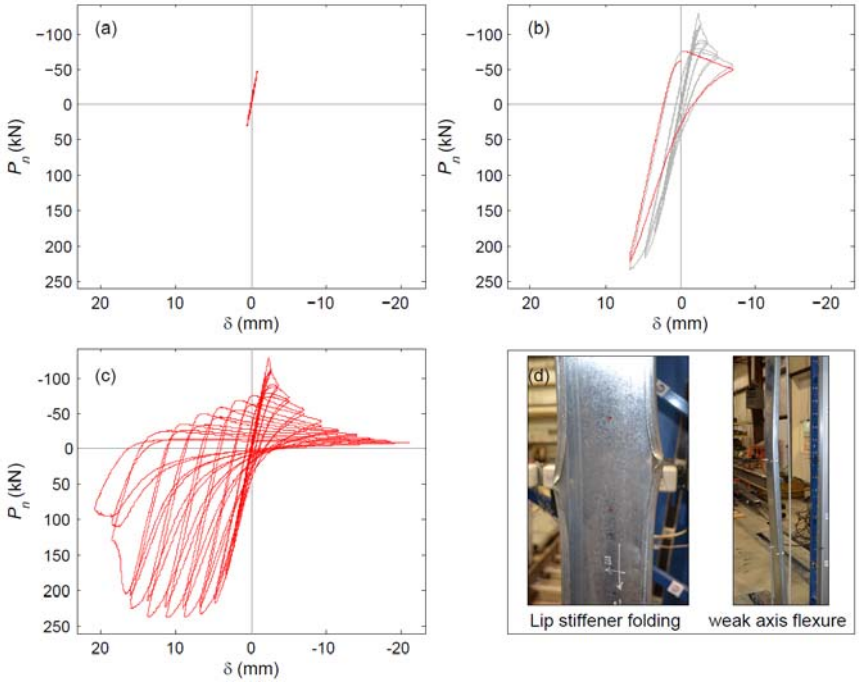

Figure 5. Cyclic load-deformation response specimen 600S137-97-GAC-1, (a) 6 cycles, (b) 20 cycles, (c) complete response, (d) failure mode.

Local buckling limit state

Cyclic response of the LAC specimens was characterized by web buckling with at least two half-waves occurring before reaching the peak compressive load. After peak load in compression, one half-wave locked around mid-height and damage accumulated there. Compressive strength and unloading stiffness then degraded quickly on the compression side as seen in Fig. 6(b-c). This deterioration was slower for the 600 specimens than for the 362 specimens. Strength in tension deteriorated faster in the 600LAC specimens than for the 362LAC specimens. The 362 specimens experienced yielding close to the rounded corners and a yield line across the web. Tearing started thereafter and propagated around the cross-section. The 600 specimens exhibited similar

behavior, but as shown in Fig. 6d, two yield lines formed around mid-height where tearing occurred. The 600LAC specimens underwent about 100 cycles after which the web was still carrying some tensile load.

The monotonic response of the LAM specimens demonstrated similar deformations as their cyclic counterpart; however, in the 362LAM specimens these deformations occurred closer to the top end plate. The 362LAM specimens also showed lower initial stiffness than their cyclic counterparts (i.e., 362S162-54-LAC specimens) as seen in Fig. 9a. In contrast, as shown in Fig. 9b the initial stiffness of the 600LAM specimens is similar to their cyclic counterpart. Both cyclic and monotonic exceeded the predicted compressive capacity P_n but reached maximum values in tension below the yield load P_y (see Table 4). It is hypothesized that for the thinner specimens (e.g., 600S162-33-LAC), the flanges and corners carried more of the tensile load than the web, and therefore the cross-section was not fully effective in tension.

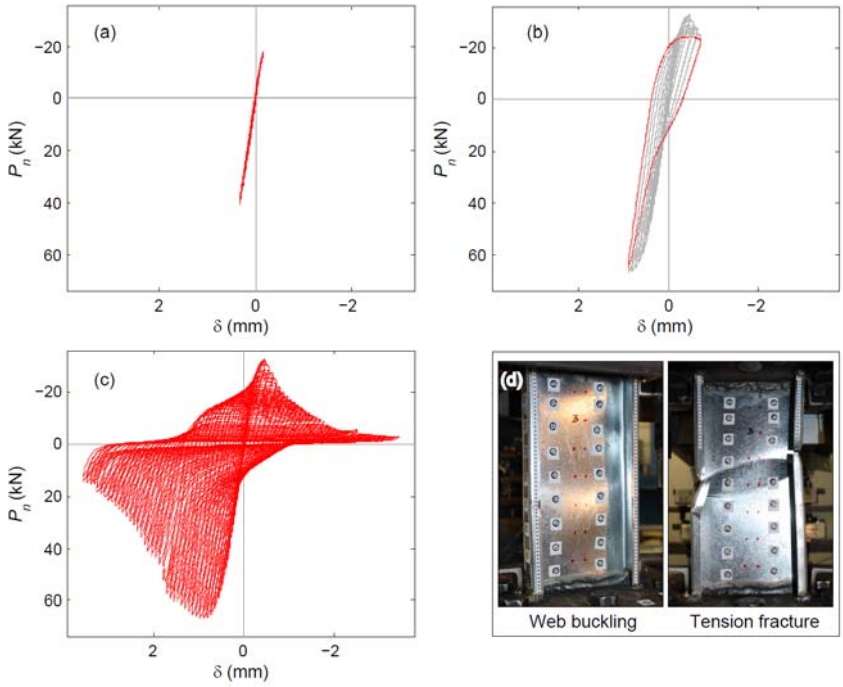

Figure 6. Cyclic load-deformation response specimen 600S162-33-LAC-2, (a) 6 cycles, (b) 20 cycles, (c) complete response, (d) failure mode.

Distortional buckling limit state

The cyclic response of the 600DAC specimens was characterized by the formation of at least one half-wavelength centered at mid-height as seen in Fig. 7d. As shown in Fig. 7(b, c), the compressive strength as well as the unloading stiffness on the compression side degraded more gradually than the in the GAC and LAC specimens. Damage accumulated from inelastic strains at the rounded corners as the member stretched and compressed. The strength in tension remained constant until tearing started at the rounded corners and propagated around the cross section. The 362DAC specimens experienced fewer cycles than the 600DAC specimens before fracture, compare 25 cycles to 50 cycles for the 362S137-68-DAC-1 and 600S137-68-DAC-1 specimens respectively. The deformations experienced by the 362DAC specimens were a combination of distortional and local buckling of the web near one of the end plates. However, web buckling deformations were more visually noticeable than opening of the flanges. The hysteretic behavior was found to be more similar to the local buckling 362LAC specimens.

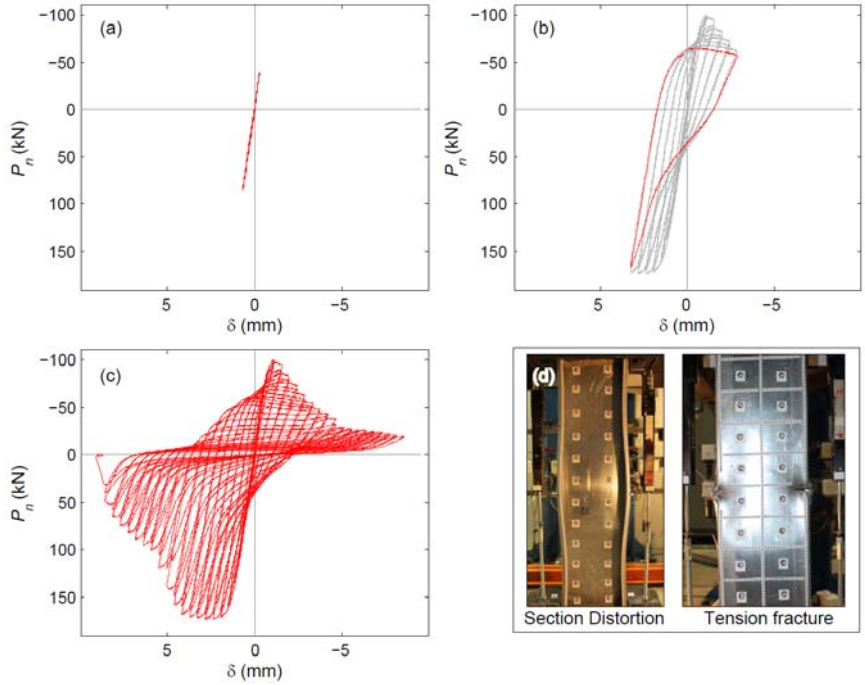

Figure 7. Cyclic load-deformation response specimen 600S137-68-DAC-2, (a) 6 cycles, (b) 20 cycles, (c) complete response, (d) failure mode.

The monotonic response of the DAM specimens exhibited similar deformations as their cyclic counterpart. Their initial stiffness however, is lower than for the DAC specimens as seen in Fig. 10. The 600 specimens exceeded the predicted capacity in compression while the 362 specimens reached values 2% to 6% lower than P_n for both cyclic and monotonic (see Table 4).

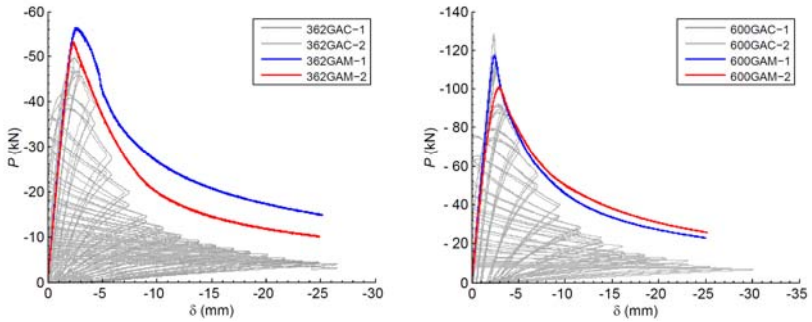

Figure 8. Global buckling monotonic response envelope, (a) 362 series, (b) 600 series

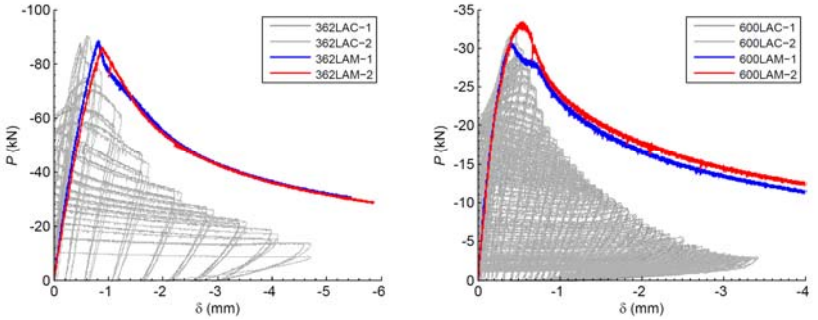

Figure 9. Local buckling monotonic response envelope, (a) 362 series, (b) 600 series

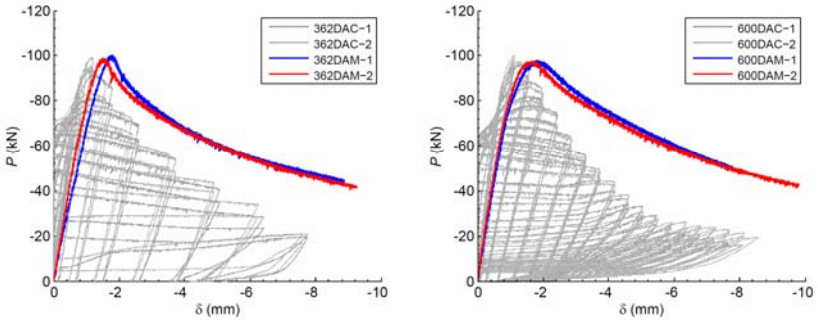

Figure 10. Distortional buckling monotonic response envelope, (a) 362 series, (b) 600 series

Discussion

Meaningful comparisons of hysteretic response across limit states are challenging to make because of the different cross-sections, specimen lengths, and buckling failure modes considered in this study. Figure 11 contrasts the hysteretic envelope for all the specimens in this study. Focusing on the compression behavior (upper right quadrant of hysteretic curve), the most important observation is that the shape of the load-deformation envelope varies with buckling mode and slenderness. Specimens with higher slenderness (e.g., 600LAC and 600DAC) have lower axial stiffness and a gradual transition through peak load into the post-buckling range, whereas specimens failing from inelastic buckling (e.g., 362LAC and 362GAC) have a sharp drop in capacity after reaching peak load as the number of cycles increase.

Figure 12 compares the normalized hysteretic energy per cycle (see inset for normalization description) as a function of cumulative axial displacement. The energy curves for the 362LAC and 362DAC specimens have the highest peaks but are the narrowest (remember that the 362DAC experienced primarily inelastic local buckling similar to the 362LAC, not distortional buckling). The high peaks mean a wider hysteretic loop and the narrow width means that energy dissipation life is relatively short. This is because tensile fracture initiated sooner in the thicker 362LAC (t=1.44 mm) and 362DAC (t=1.81 mm) when compared to the 600LAC (t=0.88 mm). The 600GAC and 362GAC specimens exhibit short narrow peaks caused by pinching of the load-deformation response when the specimen is unloaded from compression and straightens at the mid-span plastic hinge. For the local and distortional specimens, the unloading stiffness from compression to tension is higher (i.e., there is less pinching) leading to more energy dissipated per cycle.

Per cycle and total hysteretic energy dissipated per half-wavelength as a function of the cumulative axial displacement and slenderness respectively are presented in Fig. 13 and 14. This idea of normalizing hysteretic energy by buckling half-wavelength is based on the observation that after reaching peak load in compression, the tension-compression cyclic deformation was most often focused in only one half-wave. (Note that the slenderness and half-wavelength λ_ℓ and $L_{cr\ell}$ from Table 3 were used when plotting the 362DAC specimen results in Fig. 13 and 14 because their behavior in compression was most consistent with local buckling.)

Energy dissipation per half-wavelength decreased with increasing cross-

sectional slenderness as shown in Fig. 14 which is consistent with previous studies (e.g., Yao and Nikolov 1992). Specimens with higher cross-sectional slenderness (e.g., 600LAC and 600DAC) dissipated less energy per half-wavelength in a cycle (see Table 5 and Fig. 13). In contrast, specimens experiencing inelastic buckling (e.g., 362LAC and 362DAC) dissipate more energy per half-wavelength in a cycle (Fig. 13). The 362DAC dissipated by far the most cumulative energy per half-wavelength (Fig. 14 and Table 5) because the compression behavior was dominated by inelastic local buckling occurring in a relative thick base metal (t=1.81 mm). This trend demonstrates that higher base metal thicknesses dissipate more energy in local buckling. Specimens experiencing global buckling (e.g., 600GAC and 362GAC) had the lowest per cycle and cumulative energy dissipation capabilities per half-wavelength.

Table 5. Hysteretic energy dissipation

Specimen	$CHE_{0.25}$ (kN-mm)	$CHE_{0.5}$ (kN-mm)	$CHE_{1.0}$ (kN-mm)	CHE_{T} (kN-mm)	$CHE_{0.25}/L_{cr}$ (kN-mm/mm)	$CHE_{0.5}/L_{cr}$ (kN-mm/mm)	$CHE_{1.0}/L_{cr}$ (kN-mm/mm)	CHE_{T}/L_{cr} (kN-mm/mm)
600S137-97-GAC-1	12234	-	-	16063	10.70	-	-	14.05
600S137-97-GAC-2	12339	19327	-	22983	10.79	16.91	-	20.11
362S137-68-GAC-1	5676	10176	-	14952	4.97	8.90	-	13.08
362S137-68-GAC-2	5508	9078	-	10009	4.82	7.94	-	8.76
600S137-68-DAC-1	3125	6191	8234	8935	12.06	23.90	31.78	34.49
600S137-68-DAC-2	2844	5800	7598	8960	11.00	22.43	29.38	34.65
362S137-68-DAC-1	3131	5846	-	6458	44.02	82.20	-	90.81
362S137-68-DAC-2	3614	6195	-	6368	50.81	87.11	-	89.55
600S162-33-LAC-1	630	1313	2033	2550	5.64	11.75	18.19	22.82
600S162-33-LAC-2	593	1248	1863	2344	5.33	11.22	16.74	21.07
362S162-54-LAC-1	1580	3270	-	3839	22.21	45.98	-	53.98
362S162-54-LAC-2	1767	3316	-	3773	24.67	46.29	-	52.68

CHE_{xx} = cumulative hysteretic energy dissipated up to $\Sigma\delta/L$ = xx.

CHE_{T} = cumulative hysteretic energy dissipated until failure.

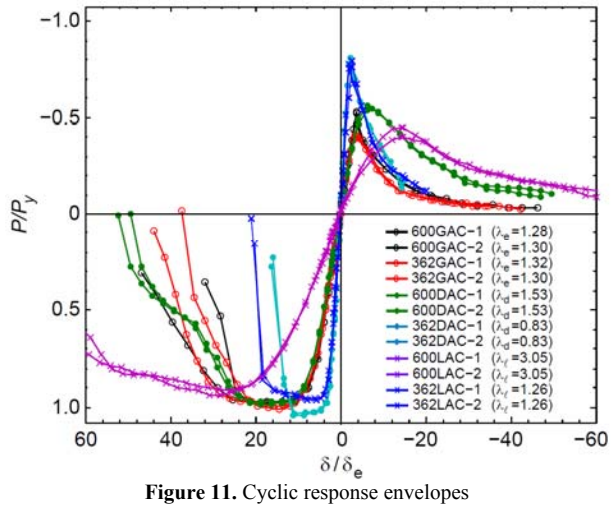

Figure 11. Cyclic response envelopes

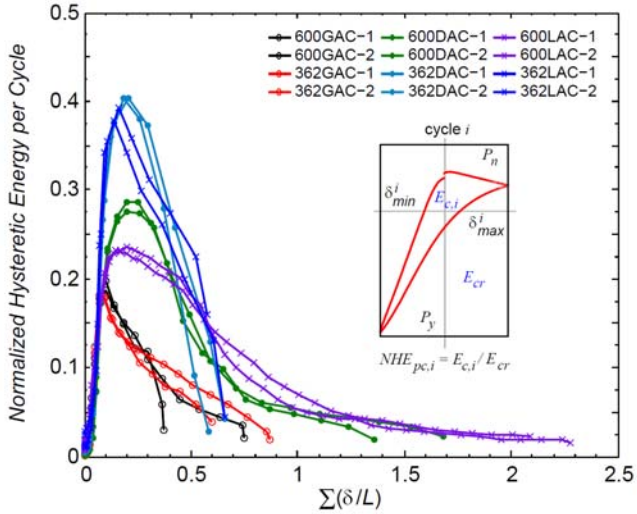

Figure 12. Normalized hysteretic energy per cycle vs. cumulative axial deformation

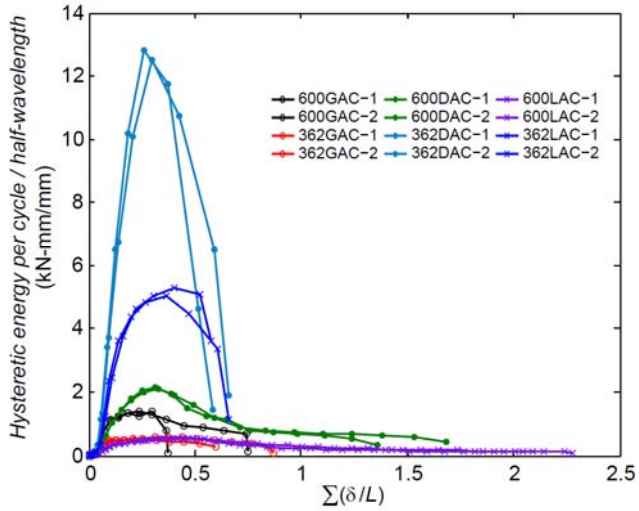

Figure 13. Hysteretic energy per cycle per half-wavelength vs. cumulative axial deformation

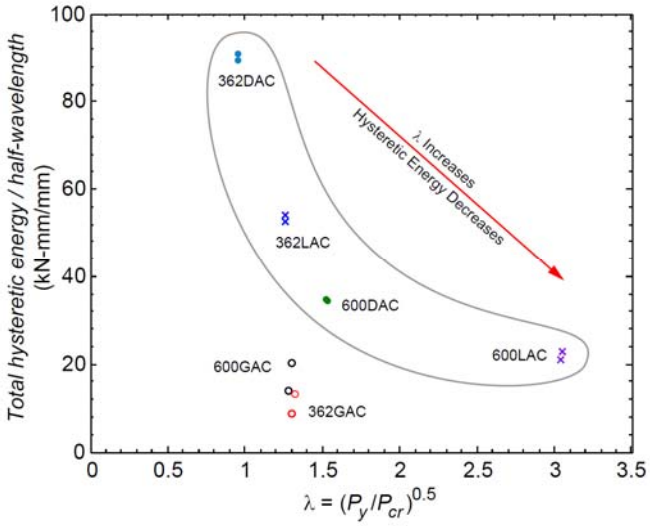

Figure 14. Total hysteretic energy per half-wavelength (CHET /Lcr) vs. cross-sectional or global slenderness

Conclusions

An experimental program was conducted to evaluate the axial cyclic response of

a cold-formed steel C-section framing members considering local, distortional, and global buckling limit states. The tests required the development of a new cyclic loading protocol for cold-formed steel members. The protocol is largely based on FEMA 461, except that the target axial displacement is calculated using elastic buckling parameters.

The observed hysteretic behavior was asymmetric because of buckling deformation in compression. For the specimens experiencing global buckling, plastic hinges formed at midspan and near the supports, and local stress concentrations resulted in tensile fracture. Specimens experiencing elastic buckling had the longest energy dissipation life. Post-buckling energy dissipation was observed that could be beneficial in an earthquake, especially for those specimens that experienced inelastic local or distortional buckling in compression.

Acknowledgements

The authors are grateful to the American Iron and Steel Institute for supporting this project, and to Clark Dietrich Building Systems for the specimen donations.

References

Ádány, S., Schafer, B.W. (2006). Buckling analysis of cold-formed steel members using CUFSM: conventional and constrained finite strip methods. 18th International Specialty Conference on Cold-Formed Steel Structures, October 26-27, 2006, Orlando, Florida.

AISI S213-07 (2007) North American Standard for Cold-Formed Steel Framing: Lateral Design. American Iron and Steel Institute, Washington, D.C. ANSI/AISI-S213-07.

AISI-S100-07 (2007) North American Specification for the Design of Cold-Formed Steel Structural Members. American Iron and Steel Institute, Washington, D.C. ANSI/AISI-S100-07.

AISI-S910-08 (2008) Test Method for Distortional Buckling of Cold-Formed Steel Hat Shaped Compression Members. American Iron and Steel Institute, Washington, D.C. ANSI/AISI-S910-08.

ASTM. (2004). E 8M-04, Standard Test Methods for Tension Testing of Metallic Materials (Metric). ASTM International, West Conshohocken, PA.

Boudreault, F.A., Blais, C., and Rogers, C.A., (2007), "Seismic Force Modification Factors for Light-Gauge Steel-Frame – Wood Structural Panel Shear Walls", Canadian Journal of Civil Engineering, 34(1), 56-65, 2007.

Bruneau, M., Uang, C. M., and Whittaker, A. S. (1998). Ductile design of steel structures. McGraw-Hill Professional.

Calderoni, B., De Martino, A., Formisano, A., and Fiorino, L. (2009). "Cold formed steel beams under monotonic and cyclic loading: Experimental investigation." Journal of Constructional Steel Research, 65(1), 219–227.

FEMA (2007) Interim protocols for determining seismic performance characteristics of

structural and nonstructural components through laboratory testing, Published by the Federal Emergency Management Agency, Document No. FEMA 461.

Goel, S. C. (1992). "Cyclic Post-Buckling Behavior of Steel Bracing Members." Stability and Ductility of Steel Structures Under Cyclic Loading. pp75-84 CRC Press.

Goggins, J. M., Broderick, B. M., Elghazouli, A. Y., and Lucas, A. S. (2006). "Behaviour of tubular steel members under cyclic axial loading." Journal of Constructional Steel Research, 62(1–2), 121-131.

Higginbotham, A. B., and Hanson, R. D. (1976). "Axial Hysteretic Behavior of Steel Members." Journal of the Structural Division, 102(7), 1365-1381.

Ikeda, K., and Mahin, S. A. (1986). "Cyclic Response of Steel Braces." Journal of Structural Engineering, 112(2), 342.

Jain, A. K., Hanson, R. D., and Goel, S. C. (1980). "Hysteretic Cycles of Axially Loaded Steel Members." Journal of the Structural Division, 106(8), 1777-1795.

Krawinkler, H. (2009). "Loading histories for cyclic tests in support of performance assessment of structural components." The 3rd International Conference on Advances in Experimental Structural Engineering, San Francisco.

Moen, C. D. (2008). Direct strength design for cold-formed steel members with perforations. Ph.D. dissertation, Johns Hopkins Univ., Baltimore.

Moncarz, P.D., and Krawinkler H. (1981) Theory and Application of Experimental Model Analysis in Earthquake Engineering, The John A. Blume Earthquake Engineering Center Report No. 50.

Nonaka, T. (1973). "An elastic-plastic analysis of a bar under repeated axial loading." International Journal of Solids and Structures, 9(5), 569-580.

Papadrakakis, M., and Loukakis, K. (1987). "Elastic-plastic hysteretic behaviour of struts with imperfections." Engineering Structures, 9(3), 162-170.

Popov, E. P., and Black, R. G. (1981). "Steel Struts under Severe Cyclic Loadings." Journal of the Structural Division, 107(9), 1857-1881.

Popov, E. P., Mahin, Stephen A, and Zayas, V. A. (1979). "Cyclic Inelastic Buckling of Thin Tubular Columns." Journal of the Structural Division, 105(11), 2261-2277.

Schafer, B.W., Nakata, N., Buonopane, S., Madsen, R. (2012). "Seismic design of multi-story cold-formed steel buildings: the CFS-NEES model building case study", 2012 ASCE Structures Congress, Chicago, IL.

Sohal, I. S., and Chen, W. F. (1988). "Local buckling and inelastic cyclic behavior of tubular sections." Thin-Walled Structures, 6(1), 63-80.

SSMA Steel Stud Manufacturers Association, Product Technical Information, ICBO ER-4943P, <http://www.ssma.com >, (December 15, 2011).

Tang, X., and Goel, S. C. (1987). "Seismic Analysis and Design Considerations of Concentrically Braced Steel Structures." Report No UMCE 87-4, Department of Civil Engineering, The University of Michigan, Ann Arbor, MI.Usami, T., and Ge, H. B. (1998). "Cyclic behavior of thin-walled steel structures—numerical analysis." Thin-Walled Structures, 32(1–3), 41-80.

Watanabe, E., Sugiura, K., Mori, T., and Suzuki, I. (1992). "Modeling of Hysteretic Behavior of Thin-Walled Box Members." Stability and Ductility of Steel Structures Under Cyclic Loading. pp225-235 CRC Press.

Yao, T., and Nikolov, P. I. (1992). "Numerical Experiment on Buckling/Plastic Collapse Behavior of Plates under Cyclic Loading." Stability and Ductility of Steel Structures

Under Cyclic Loading. pp203-214 CRC Press.
VTechWorks (2012). <http://vtechworks.lib.vt.edu> (May, 2012)